Since January 2020 Elsevier has created a COVID-19 resource centre with free information in English and Mandarin on the novel coronavirus COVID-19. The COVID-19 resource centre is hosted on Elsevier Connect, the company's public news and information website.

European Journal of Medicinal Chemistry 249 (2023) 115113

Contents lists available at ScienceDirect

European Journal of Medicinal Chemistry

journal homepage: www.elsevier.com/locate/ejmech

Research paper

Nonsteroidal anti-inflammatory drugs (NSAIDs) and nucleotide analog GS-441524 conjugates with potent *in vivo* efficacy against coronaviruses

Qifan Zhou [a,1], Yinzhu Luo [b,1], Yujun Zhu [b,1], Qishu Chen [a], Jingfei Qiu [a], Feng Cong [b,***], Yingjun Li [a,c,*], Xumu Zhang [a,**]

[a] Department of Chemistry, College of Science, Academy for Advanced Interdisciplinary Studies and Medi-X Pingshan, Southern University of Science and Technology, Shenzhen, Guangdong, 518000, China
[b] Guangdong Province Key Laboratory of Laboratory Animals, Guangdong Laboratory Animals Monitoring Institute, Guangzhou, Guangdong, 510663, China
[c] State Key Laboratory of Chemical Oncogenomics, Tsinghua Shenzhen International Graduate School, Shenzhen, 518055, China

ARTICLE INFO

Keywords:
Coronavirus
RNA dependent RNA polymerase
Nucleotide
NSAIDs
Ibuprofen
Oral antiviral agent

ABSTRACT

Coronaviruses (CoVs) infect a broad range of hosts, including humans and various animals, with a tendency to cross the species barrier, causing severe harm to human society and fostering the need for effective anti-coronaviral drugs. GS-441524 is a broad-spectrum antiviral nucleoside with potent anti-CoVs activities. However, its application is limited by poor oral bioavailability. Herein, we designed and synthesized several conjugates *via* covalently binding NSAIDs to 5′-OH of GS-441524 through ester bonds. The ibuprofen conjugate, **ATV041**, exhibited potent *in vitro* anti-coronaviral efficacy against four zoonotic coronaviruses in the *alpha*- and *beta*-genera. Oral-dosed **ATV041** resulted in favorable bioavailability and rapid tissue distribution of GS-441524 and ibuprofen. In MHV-A59 infected mice, **ATV041** dose-dependently decreased viral RNA replication and significantly reduced the proinflammatory cytokines in the liver and the lung at 3 dpi. As a result, the MHV-A59-induced lung and liver inflammatory injury was significantly alleviated. Taken together, this work provides a novel drug conjugate strategy to improve oral PK and offers a potent anti-coronaviral lead compound for further studies.

1. Introduction

Coronaviruses are positive, single-stranded, enveloped RNA viruses that infect a broad range of hosts including humans and a variety of animals with a tendency to cross the species barrier [1,2]. CoVs infect farm animals and companion animals, causing huge economic impact and loss of nonhuman companions [3,4]: such as porcine transmissible gastroenteritis virus (TGEV), porcine epidemic diarrhea virus (PEDV), canine coronavirus (CCoV), feline transmissible peritonitis virus (FIPV) of the *alpha-coronaviruses* genera; bovine coronavirus (BCoV) and equine coronavirus (ECoV) of the *beta-coronaviruses* genera; turkey coronavirus (TCoV) of the *gamma-coronaviruses* genera and porcine deltacoronavirus (PDCoV) of the *delta-coronaviruses* genera [5]. In the past two decades, three *Beta-coronavirus* have caused the prevalence of severe respiratory infections in humans, including the severe acute respiratory syndrome coronavirus (SARS-CoV, 2002), middle east respiratory syndrome coronavirus (MERS, 2012), and the recent pandemic SARS-CoV-2 (since 2019) [6,7]. The imminent threat of CoVs underscores the need for broadly active anti-coronaviral drugs for treating CoVs infection and preventing future outbreaks of novel coronaviral diseases.

Nucleos(t)ide antivirals, by directly inhibiting viral transcription and replication, are among the first-line treatment of viral disease both as a single compound and in cock-tail therapies [8,9]. The 1′-CN-4-aza-7, 9-dideazaadenosine C-nucleoside (GS-441524, **1**) and its phosphonamidite prodrug (remdesivir), are broad-spectrum antiviral nucleot(s)ide analogs across multiple virus families, including *flaviviridae*, *Filoviridae*, *Pneumoviridae*, *Paramyxoviruses*, and *Coronaviridae* [10,11]. GS-441524 is one of the few nucleotides that have potent therapeutic efficacy

* Corresponding author. Department of Chemistry, College of Science, Academy for Advanced Interdisciplinary Studies and Medi-X Pingshan, Southern University of Science and Technology, Shenzhen, Guangdong, 518000, China.
** Corresponding author.
*** Corresponding author.
E-mail addresses: congfeng521@126.com (F. Cong), liyj@sustech.edu.cn (Y. Li), zhangxm@sustech.edu.cn (X. Zhang).
[1] These authors contributed equally to this work.

https://doi.org/10.1016/j.ejmech.2023.115113
Received 17 November 2022; Received in revised form 25 December 2022; Accepted 9 January 2023
Available online 10 January 2023

against CoVs *in vivo*. Intraperitoneal injection of GS-441524 showed an up to 96% cure rate in FCoV-afflicted cats [12,13]. Previously, we showed intraperitoneal GS-441524 displays potent antiviral efficacy in SARS-CoV-2 infected Ad5-hACE2 mice and murine hepatitis virus (MHV) infected mice. However, GS-441524 displays poor oral bioavailability and aqueous solubility [14]. To solve this problem, we have developed the 5′-OH simple ester prodrug of GS-441524 which markedly improved the oral absorption of GS-441524 [15].

The concept of nucleoside ester prodrug is a well-established approach due to the high polarity and often low permeability of nucleoside [16]. This led to the approval of numerous antiviral and anticancer drugs, e. g., valganciclovir, molnupiravir and capecitabine [17]. The chosen moiety on the other side of the ester linkage was preferably to be another active agent to achieve dual-target activity. NSAIDs are analgesic, antipyretic and anti-inflammatory medications, widely used to relieve symptoms related to many conditions, including viral colds [18]. Side effects, particularly gastrointestinal ulcerogenic activity and renal toxicity, often limit their use. Therefore, introducing another pharmacophore to masking of the free carboxylic group is a promising approach to design dual-target agent. For example, nitric oxide-releasing NSAIDs, such as NO-aspirin (NCX-4016) and the ibuprofen derivative, contain a cleavable ester linker to a nitric oxide-releasing moiety was reported with a superior anti-inflammatory and antithrombotic profile [19,20].

As a continuous effort to develop GS-441524-based antivirals, here, six NSAIDs (fenoprofen, naproxen, ketoprofen, ibuprofen, diclofenac, and indomethacin) containing a free carboxylic acid was employed to esterify with the 5′-OH of GS-441524 to design novel conjugates (Fig. 1). The ester bonds are expected to be hydrolyzed *in vivo* which results in two active metabolites. On the one hand, by masking the polarized 5′-OH, the novel conjugates are expected to improve the bioavailability of GS-441524. On the other hand, the release of NSAIDs potentially get secondary effect to relieve symptoms, such as, pain, fever, and other inflammatory processes related to CoVs infection [21,22]. We reported the synthesis and antiviral potency of the conjugates against different CoVs, including murine coronavirus mouse hepatitis virus A-59 (MHV-A59), CCoV, FIPV, and TGEV. Using the model *β-coronavirus* MHV, we demonstrated that GS-441524 and ibuprofen conjugate, **ATV041**, dramatically inhibited viral replication and reduced tissue injury in the liver and lung.

2. Results

2.1. Chemistry

The synthetic route of the GS-441524 and NSAIDs conjugates (**ATV038-ATV043**) was described in Scheme 1. The 2′,3′-hydroxyl moieties of **GS-441524** were protected with acetonide by using 2,2-dimethoxypropane in the presence of *p*-TsOH to afford **2** in over 90% yield. Respectively, the carboxylic acid of fenoprofen, naproxen, ketoprofen, ibuprofen, diclofenac or indomethacin was reacted with intermediate **2** to product the corresponding esters **3a-3f** *via* *N*,*N*′-diisopropylcarbodiimide/4- (dimethylamino)pyridine (DIC/DMAP) condensation. DIC selectively coupled with the 5′-OH of GS-441524, while did not affect the 4-NH_2 group. The selectivity is better than other condensation agents after a condition screening, such as 1,3-dicyclohexylcarbodiimide (DCC) or 1-ethyl-3-(3-dimethylaminopropyl) carbodiimide (EDCI). The subsequent hydrolysis of **3a-3f** with 66.7% formic acid to obtain the target compounds **ATV038**–**043** in high yields.

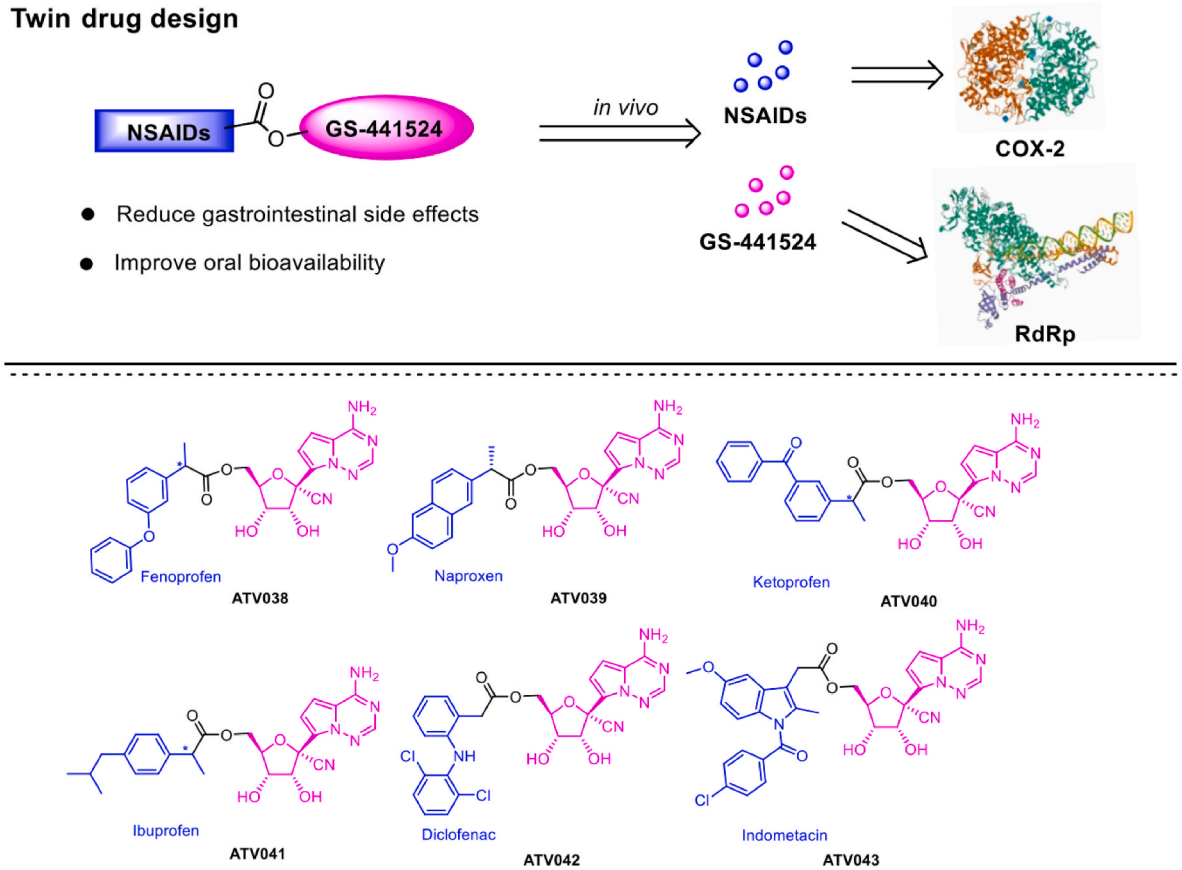

Fig. 1. Schematic diagram of oral conjugates design for the treatment of coronavirus infection and the chemical structures of designed compounds.

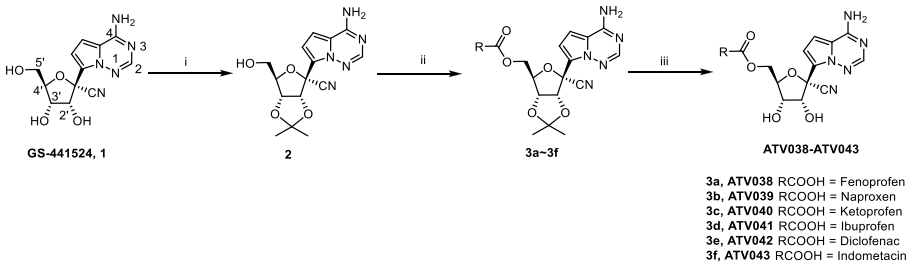

Scheme 1. Synthesis of the 5′-ester conjugates of GS-441524.
[a] Reagents and conditions: i) 2,2-Dimethoxypropane, *p*-TsOH, DCM, rt, 8 h; ii) RCOOH, DIC, DMAP, ACN, rt, 12 h; iii) HCOOH, water, 50 °C, 36 h.

2.2. The GS-441524 and NSAIDs conjugates possess potent cross-strain activities against CoVs

To evaluate the anti-CoVs activities of novel conjugates, we initially infected L929 cells with MHV-A59, a member of subgroup 2a of *β-coronavirus*, and treated them with increasing concentrations of compounds. The viral copy was determined by real-time quantitative PCR (qPCR) analysis of the *M gene* in the supernatant. As shown in Table 1, the activities of compounds were comparable to or more potent than GS-441524 except for **ATV043**. In particular, the inhibitory activities of conjugates fenoprofen (**ATV038**, half-maximum effective concentration (EC_{50}) = 1.27 μM) and ibuprofen (**ATV041**, EC_{50} = 1.15 μM) were about 8-fold more potent relative to GS-441524 (EC_{50} = 10.01 μM) and were slightly more potent than remdesivir. Subsequently, we evaluated the antiviral efficacy of **ATV041** and **ATV043** in three *alpha-CoVs* that causing serious diseases in dogs (CCoV), cats (FIPV), and pigs (TGEV), respectively, together with GS-441524 (Fig. 2). **ATV041** exhibited broad-spectrum antiviral activities against CCoV (EC_{50} = 1.406 μM), FIPV (EC_{50} = 7.34 μM) and TGEV (EC_{50} = 3.777 μM), which was more potent than GS-441524 and **ATV043**. This result indicated that introducing of ibuprofen at the 5′-OH position of GS-441524 could improve the *in vitro* anti-coronaviral potency. Ibuprofen along did not affect the cellular replication of MHV (Fig. S1), nor did its combination with remdesivir boost the inhibition of remdesivir (Fig. S2). In the physiochemical property determinations, the conjugates improved ClogP and the lipophilicity relative to GS-441524. The half-life ($T_{1/2}$) in human plasma was between 170 min and 265 min, indicating the potential to be subject to hydrolyzation by bio-enzymes over time. Their aqueous solubility differed: **ATV042** and **ATV043** are hardly soluble, **ATV038**, **ATV039**, and **ATV041** with slightly better solubility, and **ATV040** significantly improved the solubility, reaching 1073 μmol/L. These results indicated the superiority of the conjugate to improve the physiochemical properties relative to the poor reported solubility and lower ClogP of GS-441524 (see Table 1).

Table 1
The antivirus effect, the stability results in human plasma, solubility and calculated logP values of 6 compounds.

Compd.	MHV-A59 EC_{50} (μM)[a]	human plasma $T_{1/2}$ (min)	Solubility (μmol/L)	ClogP[b]
ATV038	1.27	169.31	29.0	2.671
ATV039	8.65	181.97	155	2.003
ATV040	4.17	199.18	1073	2.515
ATV041	1.15	265.04	49.9	2.761
ATV042	6.40	191.16	3.7	3.527
ATV043	10.08	170.07	0.1	3.389
GS-441524	10.01	ND[c]	ND	−1.43
Remdesivir	1.82	ND	ND	2.361

[a] The analysis of the anti MHV-A59 effect of compounds were performed in L929 cells. The data shown are the mean from two independent experiments.
[b] Octanol-water partition coefficient (logP) was calculated according to the Pharma Algorithms' AB/LogP v2.0 algorithm [23].
[c] Not determined.

2.3. Pharmacokinetic (PK) study of ATV041 in sprague-dawley (SD) rats

We next evaluated the PK profile of **ATV041** in SD rats. As shown in Table 2 and Fig. 3, **ATV041** was hydrolyzed to GS-441524 and ibuprofen *in vivo* to be the primary circulated forms in both intravenous (iv) and intragastric (po) groups. The PK parameters of the two active compounds after **ATV041** administration were determined separately. GS-441524, produced by **ATV041** hydrolyzed *in vivo*, displayed high oral bioavailability (F%) of 60.3% and a half-life ($T_{½}$) of 4.98 h. The C_{max} of 7.75 ± 1.58 μM/L was achieved 0.7 h after the oral administration, indicating its favorable blood exposure to be above the effective concentrations. Compared with the reported poor oral PK of GS-441524 dosed alone [15], the conjugate **ATV041** improved the oral exposure of GS-441524. In addition, oral **ATV041** resulted in high oral exposure of ibuprofen with bioavailability of 78% and area under curve ($AUC_{(0-\infty)}$) of 263 h*μM/L.

Next, BALB/c mice tissues were collected at 1 h after oral administration of 200 mg/kg **ATV041** to determine the tissue distribution. The metabolites GS-441524 and ibuprofen concentration in the plasma, liver, lung, and kidney were measured by chromatography/mass spectrometry/mass spectrometry (LC-MS/MS). 200 mg/kg GS-441524 single-administrated mice were used for comparison. The results demonstrated that the GS-441524 and ibuprofen, after hydrolysis from **ATV041**, were widely and quickly distributed in mice tissues (Fig. 4a). In contrast, GS-441524 concentrations of GS-441524 oral-dosed mice were about 5-fold lower than that of oral **ATV041** in all the samples (Fig. 4b). The PK data demonstrated the conjugate **ATV041** successfully resulted in favorable oral exposure and wide tissue distribution of active GS-441524 and ibuprofen (Fig. 4c).

2.4. ATV041 reduced virus replication and injury in BALB/c mice challenged with MHV-A59

Inspired by the excellent *in vitro* performance and favorable PK of **ATV041**, we then evaluated its *in vivo* efficacy in the MHV-A59 infected BALB/c mice. As shown in Fig. 5a, the mice were intranasally inoculated with a lethal dose of MHV-A59 ($TCID_{50} = 10^{-7.125}$/100 μL per mouse) and divided into 6 groups (group A, B1–B2, C1–C3). 8 mock-infected mice were used as health controls (group D). The oral treatment of therapeutic drug or vehicle starts 1 h after virus inoculation. Then mice from group A, B1–B2, and C1–C3 (4 per group) were sacrificed at 3 days post inoculation (dpi) for qPCR analysis of viral copies, histological analysis, and serum chemical analysis. The remaining mice were kept for observation until 23 dpi.

qPCR analysis in the lung and liver homogenates showed that the virus RNA copies reached high levels in both the liver and the lung at 3 dpi (Fig. 5d). The viral replication in the liver was dose-dependently inhibited by increased concentrations of **ATV041**.100 mg/kg GS-441524 (B1) and 200 mg/kg **ATV041** (C3) have the same molar concentration (34 mM/kg). They significantly inhibited the viral titers to below the detection limit. In the lungs, **ATV041** demonstrated dose-dependent inhibition of viral replication. GS-441524 alone inhibited

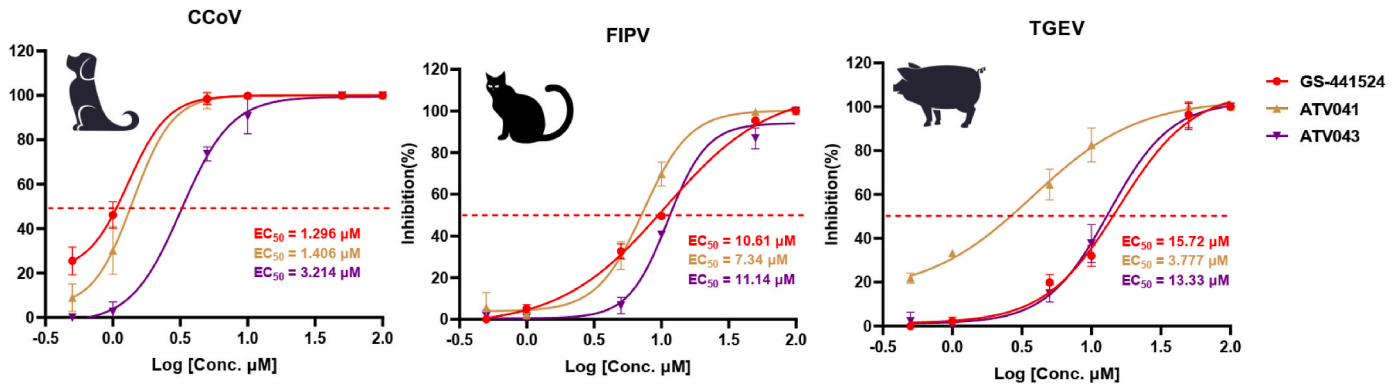

Fig. 2. Antiviral activities of GS-441524, **ATV041**, and **ATV043** against CCoV (in CRFK cells), FIPV (in CRFK cells), and TGEV (in ST cells), respectively. The EC_{50} values for each compound are indicated with the red dashed lines.

Table 2
PK parameters after single-dose of **ATV041** in SD rats[a].

Analytes	Route	Dose	$T_{1/2}$	T_{max}	C_{max}	$AUC_{(0-\infty)}$	$MRT_{(0-\infty)}$	F
		mg/kggg	h	h	μM/L	h*μM/L	h	%
GS-441524	po	25.0	4.98 ± 3.57	0.67 ± 0.29	7.75 ± 1.58	22.6 ± 2.34	3.16 ± 1.21	60.31 ± 0.06
	iv	5.0	2.81 ± 3.28	0.08 ± 0.00	5.67 ± 0.57	7.51 ± 0.85	1.28 ± 0.139	–
Ibuprofen	po	25.0	2.63 ± 1.78	0.67 ± 0.29	80.2 ± 12	263 ± 37	3.35 ± 0.925	78.42 ± 0.11
	iv	5.0	1.58 ± 0.82	0.03 ± 0.00	41.8 ± 3.12	67.1 ± 4.39	1.57 ± 0.294	–

[a] Calculation of PK parameters for GS-441524 and ibuprofen after a single po dose (25 mg/kg) or single iv dose (5 mg/kg) of **ATV041** in SD rats. Results are shown as the mean ± standard deviation (SD), n = 3.

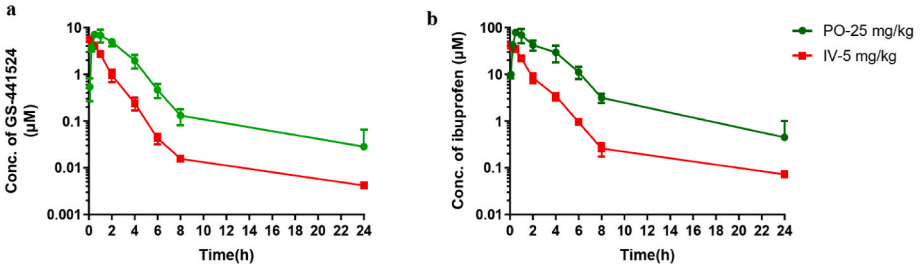

Fig. 3. Time-plasma concentration curves are shown for GS-441524 and ibuprofen following a single dose of **ATV041** in SD rats (n = 3, mean ± SD).

the viral replication by about one order of magnitude in the lungs, which was less promise than that in the liver. **ATV041** at the same molar concentration (200 mg/kg) remarkably inhibited the viral titer to blow the detection limit, demonstrating a significantly increased potency than GS-441524. Ibuprofen dosed alone did not show an antiviral effect, which was consistent with the result that ibuprofen did not inhibit MHV-A59 cellular replication up to 200 μM (Fig. S1), indicating the increased antiviral potency of **ATV041** mainly resulted from the improved oral PK of **ATV041**.

Coronaviruses infection led to the increased expression of type I interferons (IFN-α, β) and induced the expression of interferon-inducible genes and inflammatory factors, including tumor necrosis factor (TNF)-α, interleukin (IL)-6, IL-1β, IFN-γ, and C-X-C motif chemokine (CXCL10), which collaboratively force the body into an antiviral state [24,25]. However, the pro-inflammatory factor is a double-edged sword as the unregulated release may lead to cytokine storm, and excessive cytokine-mediated life-threatening inflammatory cell death (pan--apoptosis) [26]. For incidence, TNF-α and IFN-γ could induce pan-apoptosis and directly mediate T cell exhaustion, leading to lethal shock syndrome [27,28]. Thus, we tested the proinflammatory regulatory action of compounds in the lung (Fig. 5f) and the liver (Fig. 5g). In the livers, **ATV041** significantly reduced the production of key proinflammatory mediators, such as TNF-α, IL-1β, IL-6, IFN-γ, and CXCL10. Due to the suppression of virus replication in the tissues, the antiviral cytokine IFN-β was also significantly reduced. Ibuprofen alone did not obviously affect the inflammatory mediators tested here. In the lungs, **ATV041** was more potent than GS-441524 in normalizing the inflammatory factors. At the high dose of 200 mg/kg, the pro-inflammatory factors were considerably reduced to a level similar to the mock-infected mice. Representative H&E images of lung sections in MHV-infected mice indicated moderate interstitial pneumonia with thickened alveolar septa, infiltration of lymphocytes, and necrotic debris. **ATV041**-dosed mice had alleviated symptoms in the lung at 3 dpi (Fig. 6a), whereas GS-441524 did not demonstrate protect effects. Besides, MHV infections resulted in fulminant hepatitis, displaying hepatocyte necrosis and hemorrhage [29] and **ATV041** had obvious remission effects (Fig. 6b). In the serum chemical analysis, **ATV041** treatment significantly reduced the plasma alanine aminotransferase (ALT) and aspartate aminotransferase (AST), indicating the relief of acute liver injury caused by MHV-A549.

GS-441524, three doses of **ATV041** reduced mice mortality during the 23-day observation (Fig. 5c). The low dose of 10 mg/kg **ATV041** resulted in a 100% survival rate. However, the higher doses led to reduced survival, which was speculated to result from dose-related toxicity. Overall, these results demonstrated the potent *in vivo* anti-coronavirus activity of **ATV041**. The improved efficacy in the lung

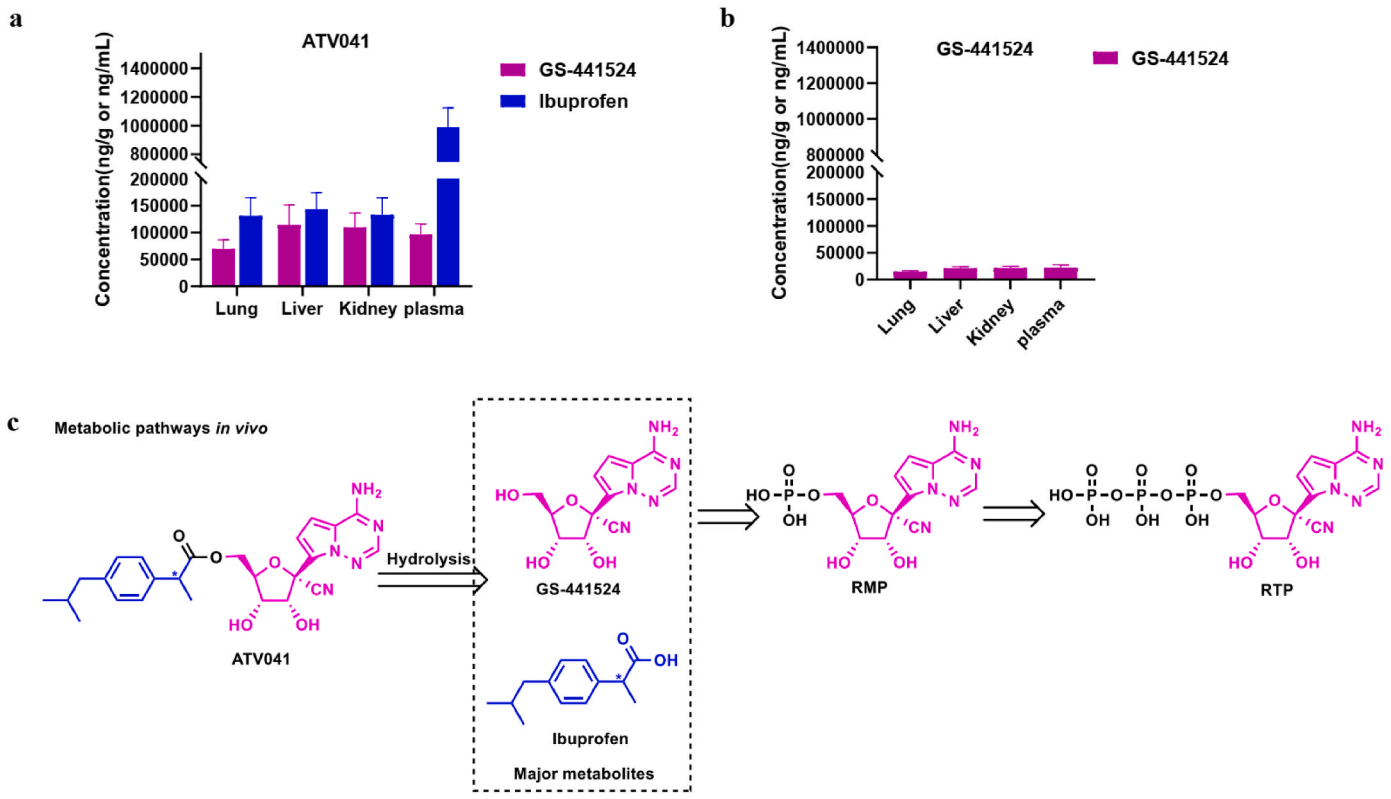

Fig. 4. Tissue distribution of compounds in BALB/c mice at 1 h after a single oral dose of **ATV041** or GS-441524. **a** The concentration of GS-441524 and ibuprofen after oral **ATV041** (200 mg/kg) in liver, lung, kidney, and plasma. **b** The concentration of GS-441524 after oral GS-441524 (200 mg/kg). n = 5 per group, Error bars indicate SEM. **c** The predicted *in vivo* metabolic pathway of **ATV041**.

was consistent with the high concentration of GS-441524 presented by **ATV041** to the lung (Fig. 4a).

3. Conclusion and discussion

Coronaviruses are among the most dangerous pathogens for human and animals, underscoring the need for discovering broad-spectrum oral anti-CoV agents. In this study, we covalently combined GS-441524 with NSAIDs *via* hydrolyzable ester bond to design conjugates with improved PK and anti-CoVs effacicy. Among the newly synthesized compounds, the ibuprofen conjugate **ATV041** was identified with potent antiviral activity against MHV-A59 in the *beta-coronavirus* subgroup. It broadly inhibited the virus replication of three *alpha-CoVs* (CCoV, FIPV, and TGEV). Meanwhile, by masking the 5′-OH polar group that impaired the absorption of GS-441524, the oral bioavailability was significantly improved as well as the distribution to tissues. Cellular GS-441524 is phosphorylated to the monophosphate (RMP) and further triphosphate (RTP) as the active form (Fig. 4c). RTP incorporates in the nascent RNA and stalls viral RNA synthesis *via* two mechanisms, as revealed from the previously studies in SARS-CoV-2 [30,31]. One is the delayed -chain-termination mechanism: the growth of RTP-incorporated RNA is impaired after the addition of the third nucleotide due to the translocation barrier raised by C1′-cyano group to the side chain of nsp12 serine-861. Consequently, the RMP at RNA 3′-end is marked by unmodified nucleotide and could partially escape from the proofreading of CoV 3′–5′ exoribonuclease (ExoN). Another is the template-dependent inhibition mechanism that the RMP in the template RNA will compromise the incorporation of the complementary UTP.

Ibuprofen is the commonly used and prescribed NSAID as an analgesic, anti-inflammatory and antipyretic. It helps to relieve the symptoms associated with viral colds. **ATV041** released ibuprofen after administration which might be benefit for relieving symptoms related to CoV infection. Hence, by shielding the carboxyl groups of ibuprofen, the side effects of gastrointestinal irritation related to ibuprofen are potentially relieved [32]. In MHV-A59 infected BALB/c mice, as one of the widely-used coronavirus models for studying virus-host interactions [33], **ATV041** presented a dose-dependent efficacy in reducing viral RNA copies in the lungs and livers, superior to that of oral GS-441524 dosed alone. It significantly relieved the liver damage and inflammation caused by MHV-A59 infection. Although the lung is not the primary target of MHV, the nasal inoculation of MHV could led to lung lesions [34,35]. **ATV041** treatment significantly reduced the pathology of viral infection, while GS-441524 was less active in the lung.

Collectively, we identified **ATV041** as a potent oral conjugate of GS-441524 and ibuprofen with favorable oral PK and potent anti-CoVs efficacy in the MHV-A59 mouse model. Noticeably, the seven known CoVs infected humans all affiliate the respiratory system. The effectiveness of **ATV041** to successfully distribute in the lungs, inhibit viral copy and relieve pulmonary lesion are clinically valuable for further studies.

4. Experimental section

4.1. Chemistry

4.1.1. General procedure

All reagents used were commercially available. Reactions were monitored by thin-layer chromatography (TLC) on glass plates coated with silica gel with a fluorescent indicator (GF254). Flash silica gel column chromatography was performed using Tsingdao silica gel (60, particle size 300–400 mesh). All the ^{1}H NMR and ^{13}C NMR spectra were recorded on a Bruker 400 MHz or 600 MHz spectrometer. Chemical shifts (d) were expressed in parts per million using tetramethylsilane as an internal reference. High-resolution mass spectra (HRMS) were measured with an Agilent Accurate-Mass Q-TOF 6530 in ESI mode

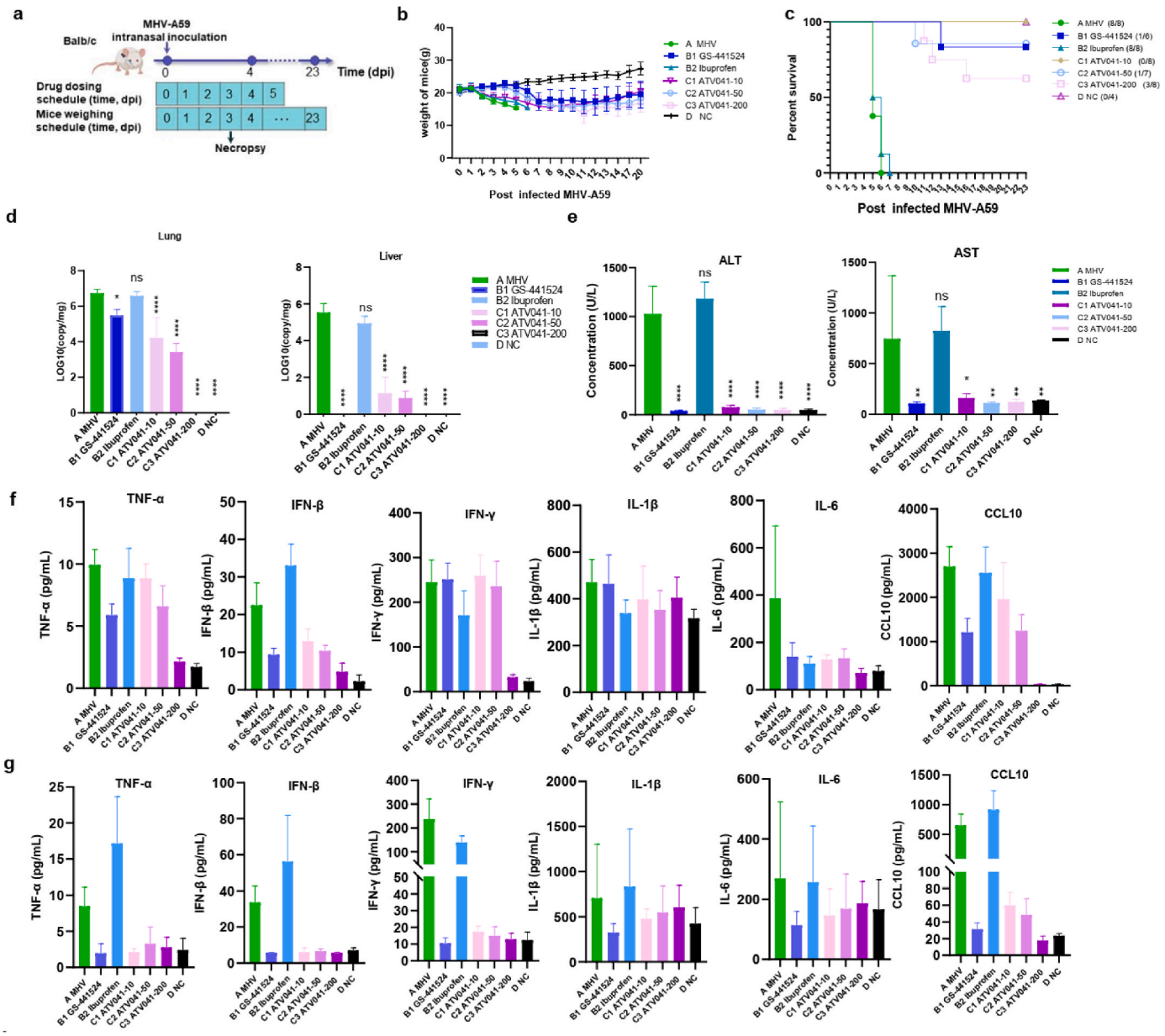

Fig. 5. The effect of **ATV041** on inhibiting viral replication and reducing inflammation in MHV-A59-infected BALB/c mice model. **a** Flowsheet of the experiment. The BALB/c mice were intranasally inoculated with MHV-A59 ($TCID_{50} = 10^{-7.125}$/100 μL per mouse) and were orally treated with vehicle (MHV, n = 12), ibuprofen (70 mg/kg (34 mM/kg), QD, n = 12), GS-441524 (100 mg/kg (34 mM/kg), QD, n = 12) or **ATV041** (10, 50 or 200 mg/kg, QD, n = 12). The normal control (NC, n = 8) was treated with vehicle (15% Cremophor EL + 82.5% PBS + 2.5% DMSO) and house together. **b** Change in body weight was measured over time. **c** The survival curve is shown. **d** The abundance of MHV-A59 *M gene* copies in mouse lungs and livers *via* qRT-PCR at 3 dpi. **e** The concentrations of ALT and AST in the serum are shown. Detection of proinflammatory cytokines in the supernatant of homogenates of lungs (**f**) and livers (**g**) at 3 dpi. QD: once daily. Error bars indicate SEM. A Kruskal-wallis test was used for statistical analysis. Data are presented as Mean ± SEM. ns, no significant difference; $^{*}P \leq 0.05$; $^{**}P \leq 0.005$; $^{***}P \leq 0.0005$; $^{****}P \leq 0.0001$.

(Agilent, Santa Clara, CA, USA). HPLC analyses were performed using a Hewlett Packard Model HP 1100 Series instruments, the compounds are at least >95% pure (OD-3; eluent, *n*-hexane/isopropanol = 70/20; flow rate 0.8 mL/min; temperature 30 °C; wavelength 254 nm; HPLC analysis data are reported in relative area % and were not adjusted to weight %).

*4.1.2. Synthesis of (3aR,4R,6R,6aR)-4-(4-aminopyrrolo[2,1-f][1,2,4] triazin-7-yl)-6-(hydroxymethyl)-2,2-dimethyltetrahydrofuro[3,4-d][1,3] dioxole-4-carbonitrile (**2**)*

To a solution of **GS-441524** (10.0 g, 0.034 mol) in dichloromethane (50 mL) was added 2,2-dimethoxypropane (22 g, 0.21 mmol) and *p*-toluenesulfonic acid (5.8 g, 0.034 mol). The mixture was stirred at room temperature until the raw material was completely consumed as monitored by TLC. The reaction was quenched with heptane (100 mL) and stirred for additional 2 h. The suspension was filtered and the filter was washed with saturated solution of sodium carbonate. After drying the product at 50 °C in the oven, intermediate **2** was obtained as a white solid (10.7 g, 95% yield). ^{1}H NMR (400 MHz, Chloroform-*d*) δ 7.93 (s, 1H), 7.08 (d, *J* = 4.6 Hz, 1H), 6.66 (d, *J* = 4.9 Hz, 1H), 5.98 (s, 2H), 5.43 (d, *J* = 6.5 Hz, 1H), 5.24 (dd, *J* = 6.6, 2.3 Hz, 1H), 4.67 (q, *J* = 1.9 Hz, 1H), 4.04–3.74 (m, 2H), 1.81 (s, 3H), 1.40 (s, 3H).

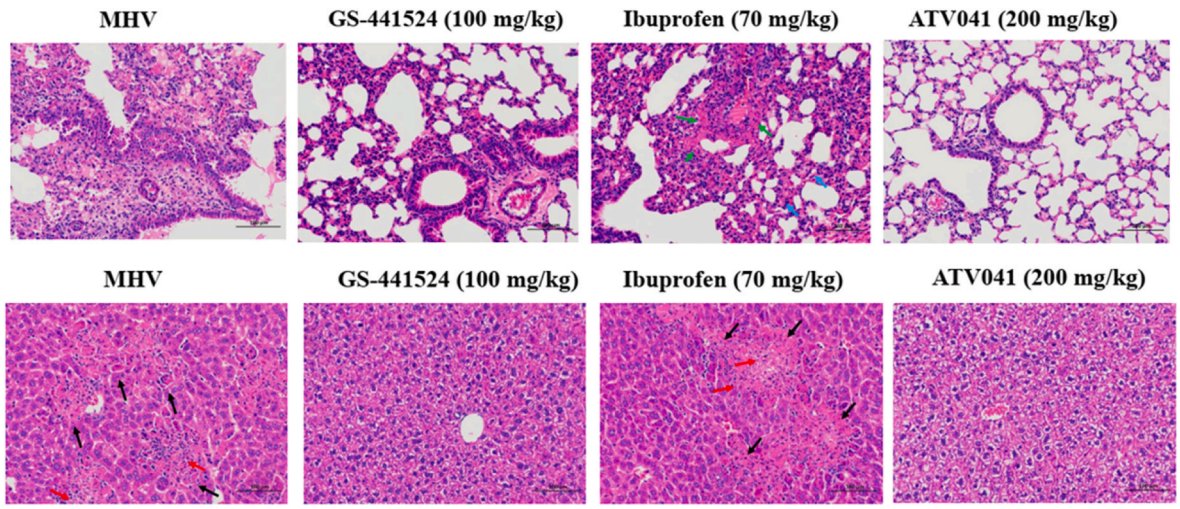

Fig. 6. Representative histopathology is shown for lungs (**a**) and livers (**b**) isolated from mice in the indicated treatment groups at 3 dpi. Scale bar: 100 μm.

*4.1.3. Synthesis of ((3aR,4R,6R,6aR)-6-(4-aminopyrrolo[2,1-f][1,2,4] triazin-7-yl)-6-cyano-2,2-dimethyltetrahydrofuro[3,4-d][1,3]dioxol-4-yl) methyl 2-(3-phenoxyphenyl)propanoate (**3a**)*

To a solution of intermediate **2** (1.0 g, 3.0 mmol), corresponding NSAIDs (3.0 mmol), 4-dimethylaminopyridine (36.6 mg, 0.3 mmol) in acetonitrile (CAN, 20 mL) was added *N*,*N*′-diisopropylcarbodiimide (0.4 g, 3.2 mmol) in dropwise. The mixture was stirred at room temperature for 12 h. The suspension was filtered and the solvent was washed with 30 mL of saturated solution of Na_2CO_3 and then with 30 mL of an aqueous solution of citric acid (20% w/v). The organic layer was dried over anhydrous Na_2SO_4. After removal of the solvent *in vacuo*, the residue was purified by column chromatography (PE/EA = 1:1). **3a** was obtained as a white solid (1.5 g, 90% yield).

*4.1.4. General procedure for preparation of compounds **ATV038~043***

((2*R*,3*S*,4*R*,5*R*)-5-(4-aminopyrrolo[2,1-*f*][1,2,4]triazin-7-yl)-5-cyano-3,4-dihydroxytetrahydrofuran-2-yl)methyl 2-(3-phenoxyphenyl) propanoate (**ATV038**).

Compound **3a** (1.5 g, 2.7 mmol) was added to a mixture of formic acid (10 mL) and water (5 mL). The reaction solution was stirred at 50 °C. After 36 h, the reaction was completed as monitored by TLC. The formic acid was removed *in vacuo*, and the resulting residue was dissolved with ethyl acetate (5 mL). Then the pH was adjusted to 7–8 with 50% Na_2CO_3 and stirred for at least 1 h at 0–5 °C. The precipitate was collected by filtration and washed with ethyl acetate to give the anomers of **ATV038** as a white solid (0.74 g, 53% yield). HPLC purity: 100%. ^{1}H NMR (600 MHz, DMSO-d_6) δ 7.94 (br, 2H), 7.90 (s, 1H), 7.45–7.24 (m, 3H), 7.18–6.81 (m, 7H), 6.71 (dd, *J* = 38.9, 4.5 Hz, 1H), 6.33 (dd, *J* = 26.5, 6.0 Hz, 1H), 5.45–5.30 (m, 1H), 4.67–4.53 (m, 1H), 4.40–4.10 (m, 3H), 3.97–3.70 (m, 2H), 3.35 (s, 3H), 1.41–1.27 (m, 3H). ^{13}C NMR (151 MHz, DMSO-d_6) δ 173.9, 173.8, 157.3, 157.2, 156.8, 156.0, 148.4, 143.1, 143.0, 130.6, 130.5, 130.5, 124.0, 123.9, 123.9, 123.0, 122.7, 119.2, 119.1, 118.1, 117.9, 117.5, 117.4, 117.0, 110.6, 101.4, 101.3, 81.7, 81.4, 79.6, 79.4, 74.5, 70.5, 65.4, 64.1, 63.8, 44.7, 19.0, 18.8. ESI-HRMS: *m/z* $[M+H]^+$ calcd for $C_{27}H_{26}N_5O_6$: 516.1883; found: 516.1876.

Compounds **ATV039~ ATV043** were synthesized using a procedure analogous to the synthesis of compound **ATV038**.

((2*R*,3*S*,4*R*,5*R*)-5-(4-aminopyrrolo[2,1-*f*][1,2,4]triazin-7-yl)-5-cyano-3,4-dihydroxytetrahydrofuran-2-yl)methyl (*S*)-2-(6-methoxynaphthalen-2-yl)propanoate (**ATV039**).

ATV039 was obtained as a white solid (0.77 g, 59% yield). HPLC purity: 99.88%. ^{1}H NMR (600 MHz, DMSO-d_6) δ 7.96 (br, 2H), 7.92 (s, 1H), 7.74–7.68 (m, 2H), 7.65 (s, 1H), 7.33 (dd, *J* = 8.5, 1.8 Hz, 1H), 7.26 (d, *J* = 2.5 Hz, 1H), 7.12 (dd, *J* = 9.0, 2.5 Hz, 1H), 6.93 (d, *J* = 4.5 Hz, 1H), 6.75 (d, *J* = 4.5 Hz, 1H), 6.24 (d, *J* = 6.1 Hz, 1H), 5.34 (d, *J* = 5.8 Hz, 1H), 4.59 (t, *J* = 5.5 Hz, 1H), 4.37 (dd, *J* = 12.1, 2.6 Hz, 1H), 4.25–4.14 (m, 2H), 3.90–3.86 (m, 2H), 3.86 (s, 3H), 1.43 (d, *J* = 7.1 Hz, 3H). ^{13}C NMR (151 MHz, DMSO-d_6) δ 173.7, 157.2, 155.6, 147.9, 135.4, 133.3, 129.1, 128.3, 127.0, 126.1, 125.6, 123.5, 118.7, 116.9, 116.6, 110.3, 105.7, 100.9, 81.4, 78.9, 74.0, 70.0, 63.3, 55.2, 44.4, 18.4. ESI-HRMS: *m/z* $[M+H]^+$ calcd for $C_{26}H_{26}N_5O_6$: 504.1883; found: 504.1876.

((2*R*,3*S*,4*R*,5*R*)-5-(4-aminopyrrolo[2,1-*f*][1,2,4]triazin-7-yl)-5-cyano-3,4-dihydroxytetrahydrofuran-2-yl)methyl 2-(3-benzoylphenyl) propanoate (**ATV040**).

The anomers of **ATV040** was obtained as a white solid (0.81 g, 62% yield). HPLC purity: 100%.^{1}H NMR (600 MHz, DMSO-d_6) δ 7.95 (br, 2H), 7.91 (s, 1H), 7.73–7.42 (m, 9H), 6.88 (dd, *J* = 9.1, 4.5 Hz, 1H), 6.69 (dd, *J* = 42.0, 4.5 Hz, 1H), 6.32 (dd, *J* = 28.4, 6.1 Hz, 1H), 5.39 (dd, *J* = 11.5, 5.9 Hz, 1H), 4.59 (dt, *J* = 23.5, 5.5 Hz, 1H), 4.43–4.14 (m, 3H), 4.00–3.78 (m, 2H), 1.45–1.34 (m, 3H). ^{13}C NMR (151 MHz, DMSO-d_6) δ 196.0, 173.9, 156.0, 148.4, 141.3, 137.7, 137.6, 137.3, 133.2, 133.1, 132.4, 132.1, 130.1, 130.0, 129.3, 129.3, 129.0, 129.0, 128.9, 123.9, 117.3, 117.0, 117.0, 110.6, 110.6, 101.4, 101.3, 81.7, 81.5, 79.5, 79.4, 74.5, 74.5, 70.5, 70.5, 64.2, 63.9, 55.4, 44.6, 19.0, 18.9. ESI-HRMS: *m/z* $[M+H]^+$ calcd for $C_{28}H_{26}N_5O_6$: 528.1883; found: 528.1877.

((2*R*,3*S*,4*R*,5*R*)-5-(4-aminopyrrolo[2,1-*f*][1,2,4]triazin-7-yl)-5-cyano-3,4-dihydroxytetrahydrofuran-2-yl)methyl 2-(4-isobutylphenyl)propanoate (**ATV041**).

The anomers of **ATV041** was obtained as a white solid (0.83 g, 60% yield). HPLC purity: 100%. ^{1}H NMR (600 MHz, DMSO-d_6) δ 7.93 (d, *J* = 1.7 Hz, 6H), 7.18–7.13 (m, 2H), 7.12–7.06 (m, 4H), 7.01 (d, *J* = 8.0 Hz, 2H), 6.93 (dd, *J* = 5.6, 4.5 Hz, 2H), 6.75 (d, *J* = 4.5 Hz, 1H), 6.67 (d, *J* = 4.5 Hz, 1H), 6.35–6.23 (m, 2H), 5.39–5.25 (m, 2H), 4.69–4.52 (m, 2H), 4.37–4.31 (m, 1H), 4.28–4.13 (m, 5H), 3.96–3.88 (m, 1H), 3.86–3.79 (m, 1H), 3.77–3.67 (m, 2H), 2.41 (d, *J* = 7.2 Hz, 2H), 2.36 (d, *J* = 7.1, 1.8 Hz, 2H), 1.85–1.64 (m, 2H), 1.42–1.26 (m, 6H), 0.88–0.69 (m, 12H). ^{13}C NMR (151 MHz, DMSO) δ 174.3, 174.2, 156.1, 156.1, 148.4, 148.4, 140.3, 140.2, 138.1, 129.6, 129.5, 127.5, 127.5, 124.0, 117.4, 117.3, 117.0, 117.0, 110.7, 110.7, 101.4, 101.4, 81.8, 81.4, 79.5, 79.4, 74.5, 70.4, 70.4, 63.8, 63.5, 44.7, 44.7, 44.6, 44.5, 30.0, 30.0, 23.8, 22.7, 22.6, 22.5, 19.1, 18.9. ESI-HRMS: *m/z* $[M+H]^+$ calcd for $C_{25}H_{30}N_5O_5$: 480.2247; found: 480.2241.

((2*R*,3*S*,4*R*,5*R*)-5-(4-aminopyrrolo[2,1-*f*][1,2,4]triazin-7-yl)-5-cyano-3,4-dihydroxytetrahydrofuran-2-yl)methyl 2-(2-((2,6-dichlorophenyl)amino)phenyl)acetate (**ATV042**).

The anomers of **ATV042** were obtained as a white solid (0.82 g, 49% yield). HPLC purity: 100%. ^{1}H NMR (600 MHz, DMSO-d_6) δ 7.97 (br, 2H), 7.94 (s, 3H), 7.52 (d, *J* = 8.1 Hz, 2H), 7.21 (t, *J* = 8.1 Hz, 1H), 7.15 (dd, *J* = 7.5, 1.6 Hz, 1H), 7.10–7.01 (m, 2H), 6.92 (d, *J* = 4.5 Hz, 1H), 6.86–6.76 (m, 2H), 6.34 (d, *J* = 6.0 Hz, 1H), 6.24 (dd, *J* = 8.1, 1.2 Hz,

1H), 5.42 (d, $J = 5.9$ Hz, 1H), 4.67 (dd, $J = 6.0$, 4.9 Hz, 1H), 4.40 (dd, $J = 11.8$, 2.4 Hz, 1H), 4.32–4.19 (m, 2H), 3.82 (s, 2H). ^{13}C NMR (151 MHz, DMSO-d_6) δ 171.9, 156.1, 148.4, 143.4, 137.5, 131.4, 131.3, 129.6, 128.3, 126.5, 123.9, 123.3, 121.0, 117.4, 117.0, 116.2, 110.8, 101.4, 81.6, 79.7, 74.4, 70.7, 64.5, 37.3. ESI-HRMS: *m/z* $[M+H]^+$ calcd for $C_{26}H_{23}Cl_2N_6O_5$: 569.1107; found: 569.1101.

((2*R*,3*S*,4*R*,5*R*)-5-(4-aminopyrrolo[2,1-*f*][1,2,4]triazin-7-yl)-5-cyano-3,4-dihydroxytetrahydrofuran-2-yl)methyl 2-(1-(4-chlorobenzoyl)-5-methoxy-2-methyl-1H-indol-3-yl)acetate (**ATV043**).

ATV043 was obtained as a white solid (0.71 g, 42% yield). HPLC purity: 99.76%. ^{1}H NMR (600 MHz, DMSO-d_6) δ 7.93 (s, 3H), 7.70–7.58 (m, 4H), 6.98 (d, $J = 2.5$ Hz, 1H), 6.94 (d, $J = 9.0$ Hz, 1H), 6.90 (d, $J = 4.5$ Hz, 1H), 6.78 (d, $J = 4.5$ Hz, 1H), 6.71 (dd, $J = 9.0$, 2.6 Hz, 1H), 6.31 (d, $J = 6.0$ Hz, 1H), 5.41 (d, $J = 5.8$ Hz, 1H), 4.69–4.61 (m, 1H), 4.43–4.32 (m, 1H), 4.30–4.21 (m, 2H), 3.95 (q, $J = 5.8$ Hz, 1H), 3.79 (s, 2H), 3.71 (s, 3H), 2.18 (s, 3H). ^{13}C NMR (151 MHz, DMSO) δ 174.3, 174.2, 156.1, 156.1, 148.4, 148.4, 140.3, 140.2, 138.1, 129.6, 129.5, 127.5, 127.5, 124.0, 117.4, 117.3, 117.0, 117.0, 110.7, 110.7, 101.4, 101.4, 81.8, 81.4, 79.5, 79.4, 74.5, 70.4, 70.4, 63.8, 63.5, 44.7, 44.7, 44.6, 44.5, 30.0, 30.0, 23.8, 22.7, 22.6, 22.5, 19.1, 18.9. ESI-HRMS: *m/z* $[M+H]^+$ calcd for $C_{31}H_{28}ClN_6O_7$: 631.1708; found: 631.1701.

4.2. Biology

4.2.1. Cells, and viruses

L929 cells were purchased from the American Type Culture Collection, Feline kidney cells (CRFK cells) and Swine testicle cells (ST cells) were stored at Guangdong Province Key Laboratory of Laboratory Animals. MHV-A59 was obtained from the American Type Culture Collection and expanded in mouse liver cells NCTC 1469. Supernatants were collected and a passage 7 stock was subsequently stored at −80 °C until used. Canine coronavirus (CCoV), Transmissible Gastroenteritis Virus (TGEV) and Infectious Peritonitis Virus (FIPV) were isolated and stored at Guangdong Province Key Laboratory of Laboratory Animals. All the virus infection experiments were performed in the BSL 2 laboratory of Guangdong Laboratory Animals Monitoring Institute. All animal studies protocols were approved by the Animal Welfare Committee and all procedures used in animal studies complied with the guidelines and policies of the Animal Care and Use Committee.

4.2.2. In vitro anti-MHV-A59, CCoV, FIPV and TGEV activity assays

L929 cells, CRFK cells and ST cells were cultured in DMEM supplemented with 10% FBS, 100 U/mL penicillin and streptomycin at 37 °C in a humidified atmosphere of 5% CO_2. The cells were seeded in 48-cell plates for 24 h to reach 80% confluence and washed thrice with serum-free medium. L929 cells were infected with MHV-A59 (0.01 MOI), CRFK cells were infected with CCoV and FIPV (0.01 MOI), ST cells were infected with TGEV (0.01 MOI) at 37 °C for 1 h. **ATV041**, ATV044, GS-441524, or DMSO were added at concentrations ranging from 0.1 μmol/L to 100 μmol/L, respectively. DMSO was set as the blank control. After incubating at 37 °C for 48 h, cells and supernatants were harvested to determine viral loads by using qRT-PCR. The inhibition rate of analogs was calculated based on the viral copy number, and the 50% effective concentration (EC_{50}) was calculated with Graphpad Prism software 8.0.

4.2.3. qRT-PCR analysis

For the detection of cellular viruses and tissue viruses, total RNA was isolated from cells or tissue samples with TRIzol reagent under the instruction of the manufacturer as previous reported [36]. The mRNAs were reverse transcribed into cDNA by PrimeScript RT reagent Kit (Takara). The cDNA was amplified by a fast two-step amplification program using ChamQ Universal SYBR qPCR Master Mix (Vazyme Biotech Co., Ltd) or Taq Pro HS Universal Probe Master Mix (Vazyme Biotech Co., Ltd). GAPDH was used to normalize the input samples *via* the ΔCt method. The relative mRNA expression level of each gene was normalized to GAPDH housekeeping gene expression in the untreated condition, and fold induction was calculated by the ΔΔCT method relative to those in untreated samples. The qRT-PCR primers are listed in Table S1.

4.2.4. Pharmacokinetic study in SD rats

Male SD rats (n = 3) were fasted for 12 h before drug administration [37]. **ATV041** was administered intravenously at 5 mg/kg or intragastrically at 25 mg/kg. Blood samples were collected from the jugular vein into anticoagulant EDTA-K2 tubes at 0.083, 0.25, 0.5, 1, 2, 3, 4, 6, 8 and 24 h for the iv group, and 0.25, 1, 0.5, 2, 3, 4, 6, 8, and 24 h for the po group, respectively. All samples were centrifuged under 4000 rpm/min for 10 min at 4 °C and the plasma (supernatants) were collected and stored at −65 °C for future analysis. An aliquot of 50 μL of each plasma sample was treated with 250 μL of acetonitrile. The samples were centrifuged under 4000 rpm/min for 10 min and filtered through 0.2 μm membrane filters. The concentration of analytes in each sample was analyzed by LC/MS/MS. PK parameters were determined following a noncompartmental analysis of the plasma concentration−time data by using Phoenix WinNonlin7.0. The following PK parameters are reported: clearance (CL; L/h/kg), the volume of distribution at steady state (Vss; L/kg), terminal half-life (T1/2; h), maximum concentration (Cmax; μM), and area under the concentration−time curve from time 0 to infinity (AUCinf; μM·h).

4.2.5. Tissue distribution

10 male BALB/c mice were randomly divided into two groups. All rats were intragastrically administered with a single dose of 200 mg/kg **ATV041** (n = 5) or 200 mg/kg GS-441524 (n = 5). At 1 h post-dosing, the mice were anesthetized, and tissues including kidney, liver, lung, and plasma were harvested. Blood samples were collected and centrifuged to obtain the plasma. All the samples were stored at −80 °C for further use. Tissue samples were individually homogenized, and the concentrations of the key metabolite GS-441524 and ibuprofen in plasma and tissue homogenates were analyzed by LC-MS/MS using the similar method as previously described [15].

4.2.6. Mouse MHV efficacy study

Specific-pathogen-free (SPF) male BALB/c mice (3–4 weeks) were anesthetized by respiratory with isoflurane and received an intranasal inoculation of 30 μL MHV-A59 ($TCID_{50} = 10^{-7.125}$/100 μL) in phosphate-buffered saline (PBS). Then the infected mice were randomly divided into 6 group (Group A, B1∼B2, C1∼C3): vehicle (n = 12), GS-441524 (B1, 100 mg/kg, QD), ibuprofen (B2, 70 mg/kg, QD), or **ATV041** (10 mg/kg (B5), 50 mg/kg (B6) or 200 mg/kg (B7), QD). Each group has 12 animals. Drugs were dissolved in the vehicle containing 15% Cremophor EL, 82.5% PBS, and 2.5% DMSO. The oral administration indicated drugs or vehicle started at 1 hpi and continuous for four days. Mock-infected mice (group D) were treated with vehicle. Mice were monitored daily for symptoms of disease: including body weights, clinical symptoms, and death for 23 days. 4 mice of each group were sacrificed at 3 dpi to collect lung and liver tissues for qRT-PCR testing, proinflammatory cytokines test, and histopathologic examination, and the plasma was taken for AST and ALT analysis.

4.2.7. AST/ALT assay

Blood from mice euthanized at 3 dpi was incubated at room temperature to allow coagulation and then centrifuged to obtain serum; the serum level of alanine transaminase (ALT) and aspartate aminotransferase (AST) were measured by using Clinical Chemistry Analyzer MS-480.

4.2.8. ELISA assay for cytokines profiles

0.1 g mice lung or liver tissue samples were added 0.9 mL double distilled water and homogenized at 60 Hz for 60 s under 4 °C. After centrifuging under 5000 rpm for 15min, the supernatants were

transferred to a clean tube. The inflammatory cytokines in the supernatants were determined. Mouse IFN-beta were determined by using Quantikine ELISA kit (MIFNB0, R&D Systems) and mouse TNF-α, IFN-γ, IL-1β, IL-6, and CXCL10 were determined by using premixed multi-analyte kit (LXSAMSM-05, R&D Systems) according to the manufacturer's protocol. The optical density of assay wells was determined by using a microplate reader set to 450 nm and the concentration at each well was calculation according to the serial diluted standards.

4.2.9. Hematoxylin and eosin staining

Lung and liver dissections were fixed in zinc formalin and embedded with paraffin. Tissue sections (~4 μm) were stained with hematoxylin and eosin for histopathologic examination. Sections were visualized under microscopy (ECLIPSE Ci-L, Nikon). Representative images were taken at 200 × and 400 × . (Wuhan servicebio technology Co., Ltd).

4.2.10. Statistical analysis

Quantitative experiments were indicated as the means ± SDs or means ± SEMs. A log-rank test, one-way analysis of variance (ANOVA) with Kruskal-wallis's correction was used for statistical analysis in Fig. 5 and respective details are indicated in the figure legends. *P* values less than 0.05 was considered statistically significant.

Declaration of competing interest

The authors declare that they have no known competing financial interests or personal relationships that could have appeared to influence the work reported in this paper.

Data availability

Data will be made available on request.

Acknowledgments

This work was supported by the National Natural Science Foundation of China (grant #82150206), National Natural Science Foundation of China Youth Program (grant #32000360, #82204194), Shenzhen Science and Technology Program (grant #JSGG20210901145403012, #JCYJ20220530113609021), Science and Technology Program of Guangzhou, China (grant #202102080304) and Guangdong Education department (grant #2022KTSCX107).

Appendix A. Supplementary data

Supplementary data to this article can be found online at https://doi.org/10.1016/j.ejmech.2023.115113.

References

[1] J.F.W. Chan, K.K.W. To, H. Tse, D.Y. Jin, K.Y. Yuen, Interspecies transmission and emergence of novel viruses: lessons from bats and birds, Trends Microbiol. 21 (2013) 544–555, https://doi.org/10.1016/j.tim.2013.05.005.
[2] S.R. Weiss, J.L. Leibowitz, Coronavirus pathogenesis, Adv. Virus Res. 81 (2011) 85–164, https://doi.org/10.1016/b978-0-12-385885-6.00009-2.
[3] A.E. Stout, N.M. André, J.A. Jaimes, J.K. Millet, G.R. Whittaker, Coronaviruses in cats and other companion animals: where does SARS-CoV-2/COVID-19 fit? Vet. Microbiol. 247 (2020), 108777 https://doi.org/10.1016/j.vetmic.2020.108777.
[4] M. Khamassi Khbou, M. Daaloul Jedidi, F. Bouaicha Zaafouri, M. Benzarti, Coronaviruses in farm animals: epidemiology and public health implications, Vet. Med. Sci. 7 (2021) 322–347, https://doi.org/10.1002/vms3.359.
[5] H. Turlewicz-Podbielska, Pomorska-Mól, M. Porcine Coronaviruses, Overview of the state of the art, Virol. Sin. 36 (2021) 833–851, https://doi.org/10.1007/s12250-021-00364-0.
[6] P.A. Rota, et al., Characterization of a novel coronavirus associated with severe acute respiratory syndrome, Science 300 (2003) 1394–1399, https://doi.org/10.1126/science.1085952.
[7] R. Lu, et al., Complete genome sequence of Middle East respiratory syndrome coronavirus (MERS-CoV) from the first imported MERS-CoV case in China, Genome Announc. 3 (2015), https://doi.org/10.1128/genomeA.00818-15.
[8] A.J. te Velthuis, Common and unique features of viral RNA-dependent polymerases, Cell. Mol. Life Sci. 71 (2014) 4403–4420, https://doi.org/10.1007/s00018-014-1695-z.
[9] S. Venkataraman, B. Prasad, R. Selvarajan, RNA dependent RNA polymerases: insights from structure, function and evolution, Viruses 10 (2018), https://doi.org/10.3390/v10020076.
[10] M.K. Lo, et al., GS-5734 and its parent nucleoside analog inhibit Filo-, Pneumo-, and Paramyxoviruses, Sci. Rep. 7 (2017), 43395, https://doi.org/10.1038/srep43395.
[11] R.L. Gottlieb, et al., Early remdesivir to prevent progression to severe covid-19 in outpatients, N. Engl. J. Med. 386 (2022) 305–315, https://doi.org/10.1056/NEJMoa2116846.
[12] P.J. Dickinson, et al., Antiviral treatment using the adenosine nucleoside analogue GS-441524 in cats with clinically diagnosed neurological feline infectious peritonitis, J. Vet. Intern. Med. 34 (2020) 1587–1593, https://doi.org/10.1111/jvim.15780.
[13] B.G. Murphy, et al., The nucleoside analog GS-441524 strongly inhibits feline infectious peritonitis (FIP) virus in tissue culture and experimental cat infection studies, Vet. Microbiol. 219 (2018) 226–233, https://doi.org/10.1016/j.vetmic.2018.04.026.
[14] Y.J. Li, et al., Remdesivir metabolite GS-441524 effectively inhibits SARS-CoV-2 infection in mouse models, J. Med. Chem. 65 (2022) 2785–2793, https://doi.org/10.1021/acs.jmedchem.0c01929.
[15] L. Cao, et al., The adenosine analog prodrug ATV006 is orally bioavailable and has preclinical efficacy against parental SARS-CoV-2 and variants, Sci. Transl. Med. 14 (2022), eabm7621, https://doi.org/10.1126/scitranslmed.abm7621.
[16] H. Sinokrot, T. Smerat, A. Najjar, R. Karaman, Advanced prodrug strategies in nucleoside and non-nucleoside antiviral agents: a review of the recent five years, Molecules 22 (2017), https://doi.org/10.3390/molecules22101736.
[17] Rautio, J. et al. Prodrugs: Design and Clinical Applications.
[18] M. Ahmadi, S. Bekeschus, K.D. Weltmann, T. von Woedtke, K. Wende, Non-steroidal anti-inflammatory drugs: recent advances in the use of synthetic COX-2 inhibitors, RSC Med Chem 13 (2022) 471–496, https://doi.org/10.1039/d1md00280e.
[19] M. Di Napoli, F. Papa, NCX-4016 NicOx, Curr. Opin. Invest. Drugs 4 (2003) 1126–1139.
[20] M.L. Lolli, et al., A new class of ibuprofen derivatives with reduced gastrotoxicity, J. Med. Chem. 44 (2001) 3463–3468, https://doi.org/10.1021/jm0108799.
[21] Centers for Disease Control and Prevention. https://www.cdc.gov/coronavirus/2019-ncov/your-health/treatments-for-severe-illness.html.
[22] S.Y. Kim, Y.J. Chang, H.M. Cho, Y.W. Hwang, Y.S. Moon, Non-steroidal anti-inflammatory drugs for the common cold, Cochrane Database Syst. Rev. (2015), https://doi.org/10.1002/14651858.CD006362.pub4. Cd006362.
[23] Y. Li, et al., Design and synthesis of tetrazole- and pyridine-containing itraconazole analogs as potent angiogenesis inhibitors, ACS Med. Chem. Lett. 11 (2020) 1111–1117, https://doi.org/10.1021/acsmedchemlett.9b00438.
[24] J.M. Gonzalez-Navajas, J. Lee, M. David, E. Raz, Immunomodulatory functions of type I interferons, Nat. Rev. Immunol. 12 (2012) 125–135, https://doi.org/10.1038/nri3133.
[25] R. Channappanavar, S. Perlman, Pathogenic human coronavirus infections: causes and consequences of cytokine storm and immunopathology, Semin. Immunopathol. 39 (2017) 529–539, https://doi.org/10.1007/s00281-017-0629-x.
[26] R. Karki, T.D. Kanneganti, The 'cytokine storm': molecular mechanisms and therapeutic prospects, Trends Immunol. 42 (2021) 681–705, https://doi.org/10.1016/j.it.2021.06.001.
[27] R. Karki, et al., Synergism of TNF-alpha and IFN-gamma triggers inflammatory cell death, tissue damage, and mortality in SARS-CoV-2 infection and cytokine shock syndromes, Cell 184 (2021) 149–168, https://doi.org/10.1016/j.cell.2020.11.025, e117.
[28] B. Diao, et al., Reduction and functional exhaustion of T cells in patients with coronavirus disease 2019 (COVID-19), Front. Immunol. 11 (2020) doi:ARTN 82710.3389/fimmu.2020.00827.
[29] H. Peng, et al., A soluble DR5-Fc chimeric protein attenuates inflammatory responses induced by coronavirus MHV-A59 and SARS-CoV-2, J. Med. Virol. 94 (2022) 5574–5581, https://doi.org/10.1002/jmv.28021.
[30] G. Kokic, et al., Mechanism of SARS-CoV-2 polymerase stalling by remdesivir, Nat. Commun. 12 (2021) 279, https://doi.org/10.1038/s41467-020-20542-0.
[31] E.P. Tchesnokov, et al., Template-dependent inhibition of coronavirus RNA-dependent RNA polymerase by remdesivir reveals a second mechanism of action, J. Biol. Chem. 295 (2020) 16156–16165, https://doi.org/10.1074/jbc.AC120.015720.
[32] A.H. Soll, D. McCarthy, NSAID-related gastrointestinal complications, Clin. Cornerstone 1 (1999) 42–56, https://doi.org/10.1016/s1098-3597(99)90088-1.

[33] N. DeAlbuquerque, et al., Murine hepatitis virus strain 1 as a model for severe acute respiratory distress syndrome (SARS), Adv. Exp. Med. Biol. 581 (2006) 373–378, https://doi.org/10.1007/978-0-387-33012-9_66.
[34] J.L. Leibowitz, et al., Genetic determinants of mouse hepatitis virus strain 1 pneumovirulence, J. Virol. 84 (2010) 9278–9291, https://doi.org/10.1128/jvi.00330-10.
[35] Z. Yang, et al., Coronavirus MHV-A59 infects the lung and causes severe pneumonia in C57BL/6 mice, Virol. Sin. 29 (2014) 393–402, https://doi.org/10.1007/s12250-014-3530-y.
[36] W. Yang, et al., Pyrazole-4-Carboxamide (YW2065): a therapeutic candidate for colorectal cancer via dual activities of wnt/beta-catenin signaling inhibition and AMP-activated protein kinase (ampk) activation, J. Med. Chem. 62 (2019) 11151–11164, https://doi.org/10.1021/acs.jmedchem.9b01252.
[37] Y. Li, et al., N-(3-Ethynyl-2,4-difluorophenyl)sulfonamide derivatives as selective raf inhibitors, ACS Med. Chem. Lett. 6 (2015) 543–547, https://doi.org/10.1021/acsmedchemlett.5b00039.